

Comparative Studies of RANS versus LES for Fan-intake Interaction

Yunfei Ma

PhD candidate

Department of Engineering

University of Cambridge

United Kingdom, CB2 1PZ

Email: ym324@cam.ac.uk

Nagabhushana Rao Vadlamani

Assistant Professor

Department of Aerospace Engineering

Indian Institute of Technology (IIT) Madras

Chennai 600036, India

Email: nrv@iitm.ac.in

Jiahuan Cui *

Assistant Professor

School of Aeronautics and Astronautics

ZJU-UIUC Institute

Zhejiang University

People's Republic of China, 310007

Email: jiahuancui@intl.zju.edu.cn

Paul Tucker

Professor

Department of Engineering

University of Cambridge

United Kingdom, CB2 1PZ

Email: pgt23@cam.ac.uk

The present research applied a mixed-fidelity approach to examine the fan–intake interaction. Flow separation induced by a distortion generator (DG) is either resolved using Large Eddy Simulation (LES) or modeled using the standard $k - \omega$ model, SA model, etc. The Immersed Boundary Method with Smeared Geometry (IBMSG) is employed to represent the effect of

*Address all issues to this author.

the fan and a wide range of test cases is studied by varying the (a) height of the DG and (b) proximity of the fan to the DG. Comparisons are drawn between the LES and the RANS approaches with/without the fan effect. It is found that in the "absence of fan", the discrepancies between RANS and LES is significant within the separation and reattachment region due to the well-known limitations of the standard RANS models. "With the fan installed", the deviation between RANS and LES decreases substantially. It becomes minimal when the fan is closest to the distortion generator. It implies that with an installed fan, the inaccuracies of the turbulence model are mitigated by the strong flow acceleration at the casing due to the fan. More precisely, the mass flow redistribution due to the fan has a dominant primary effect on the final predictions and the effect of turbulence model becomes secondary, thereby suggesting that high fidelity eddy resolving simulations provide marginal improvements to the accuracy for the installed cases, particularly for the short intake-fan strategies with fan getting closer to intake lip.

1 Introduction

To achieve higher bypass and lower fan pressure ratios, larger intakes are deployed in modern aircraft engines as compared to conventional designs. Drag penalties due to an increase in the turbulent wetted area on such large intakes is compensated by making the intake length shorter; shorter intakes result in an increased interaction between the downstream fan and the boundary layers developing over the intake. During the aircraft landing process, the rotational speed of an engine is much lower (usually by around 65%) than the design speed and the flow is prone to separation over the intake lip under these conditions. Specifically, for smaller intakes, the distortion generated by the separated flow can result in a serious deterioration of the fan performance and may even damage the engine compressor [1]. Under higher angles of attack, the extent of the distortion can almost reach the intake radius [2]. Even under moderate angles of attack, Defoe [3] found that when the flow chokes within the intake, the boundary layers can be extended by up to a third of the inlet radius.

The literature concerning both numerical and experimental studies has examined the fan–intake interaction. The numerical investigations applied the conventional Reynolds-averaged Navier–Stokes (RANS) or unsteady RANS (URANS) approaches and revealed the general flow features within blade passages [4–6]. Experimental tests [7–9] for inlet distortion and fan performance provide details of the flow features which may be used for validation of the simulations. Among these works, Wartzek [10] investigated distortion patterns in a transonic compressor stage and found that the distorted flow from the inlet can cause a global alteration in the downstream fan behavior. To investigate the influence of the fan on the distortion, Cao et al. [11] and Mauro Carnevale [12] developed a range of models aimed at reducing the cost of full, three-dimensional (3D) computational fluid dynamics (CFD) simulations. Cao et al. [11] demonstrated that the fan can accelerate the flow near the casing, thereby redistributing the mass flow. The altered distribution may either alleviate the distortion or entirely suppress the separation, depending on the proximity of fan.

Although the conventional RANS/unsteady RANS approaches are useful to capture the relevant flow physics in the general sense, the accuracy of these models is questionable, especially for largely separated flows (see [13–16]). Tyacke [17] investigated flows in different

zones of turbines and found that eddy resolving methods provided the physics in more detail and reliable data than RANS/URANS for improving fan and intake designs. Tucker and Liu [18] studied the separation region downstream of a cylinder using different RANS models (Spalart Allmaras (SA), $v_t - L, k - l, k - \epsilon, k - \omega$) and found that the eddy viscosity models can deviate by more than two orders of magnitude. By contrast, eddy resolving simulations such as Direct Numerical simulation (DNS), Large Eddy Simulation (LES) and hybrid RANS–LES have been demonstrated to yield much more consistent results (see [19–21]). However, due to its high computational cost [22], LES with a mesh-resolved fan is not yet feasible. To reduce the mesh size, some approaches, such as the Body Force Modeling approach [23], the Fan Similarity Model [12] and CFD-based throughflow models [24–27], were developed to model the geometry of fan. Their basic ideas are quite similar, distributing blade force into each fluid particles within blade regions. The differences are the ways of establishing force models, by feedback control theories or by entropy relations, which have different requirements for CFD schemes. These approaches present very promising flow features in the scenario of fan-distortion interaction. However, most simulations are based on RANS and for a higher fidelity simulation, Ma applied a mixed-fidelity modeling [28,29] using LES and fan modeling approach (IBMSG). This modeling approach is shown to accurately predict the redistribution of the mass flow upstream of the fan face. However, the degree of discrepancy between RANS and LES is still unclear. Indeed, many researchers have pointed out the reason for this discrepancy itself. For example, this comes from eddy-viscosity based closures, which performs very poor in severe separation region [30]. Details for the RANS failure in flow separation and re-attachment were also analyzed by Iaccarino et al [31]. Craft [32] also revealed that this discrepancy resulted from significant streamline curvature. But this discrepancy, if the downstream fan enacts strong flow acceleration [28], can be significantly reduced or even eliminated. This means that RANS can achieve the same satisfying performance compared to LES, and that eddy resolving methods and hence the enormous computing resources can be avoided.

Hence, the objective of the current study is to investigate the discrepancies between RANS and LES in the presence of a downstream fan with varying proximity to the distortion generator. The present research compares the predictions from the mixed-fidelity approach (LES-IBMSG)

introduced in [28, 29] with the low-fidelity models (RANS-IBMSG) in the context of fan–intake interaction. The separated flow past a distortion generator (DG) is either resolved using LES or modeled using the standard RANS models ($k - \omega$ and SA). Comparisons are drawn between LES-IBMSG/RANS-IBMSG for a wide range of test cases in which the acceleration due to the fan is altered. This is achieved by varying the (a) proximity of the fan to the DG and (b) height of the DG. The paper is organized as follows: Section 2 introduces the mixed-fidelity method and the test cases. Section 3 validates the method on a transonic rotor against experimental data. Section 4 investigates the discrepancies between RANS and LES for cases both with and without the fan. The former cases consider the effects of both the fan location and the degree of distortion. The causes of the discrepancies between the modeling approaches and their relation to the flow acceleration are studied and concluding remarks are provided in the final section.

2 Methodologies

2.1 Case set-up

The influence of flow acceleration on the prediction of separated flows is investigated via a 30° sector extracted from the Darmstadt Transonic Rotor [7–9]. This case is run with a 65% rotational speed (1361.31rad/s, equivalent to a landing speed) and a 10.6kg/s mass flow rate (the peak efficiency point). It employs a periodic boundary condition in the circumferential direction. According to the recommended spanwise scale [33] for a wall-resolved LES case, the circumferential extent (30°) is sufficient to accommodate all of the turbulence models. A radial equilibrium boundary condition is applied at the outlet, whereas the total pressure and total temperature are fixed at the inlet. Since the interest of this work is in the separated flow on the casing (the lower wall), we simply use an inviscid upper wall in order to reduce the computational cost. This nonetheless ensures that the pressure distribution at the spinner is well represented.

To generate representative inflow distortions, Reid [34] proposed various distortion generators. He also investigated the sector angle of distortion as well as the axial distance between the distortion generator and the rotor. For the present case, we adopt the distortion generator

proposed by Haug et al. [35]. This is a beveled beam with a radial extent equal to 10% of the channel height and a circumferential extent of 120° that has been designed for the investigation of fan–intake interaction on the Darmstadt Transonic Rotor. The beam has a height of ' $H = 0.02m$ ' and a length of ' $1.5H$ '. As Haug noted [35], these dimensions are able to meet both the numerical and experimental requirements and represent the distortion observed in a real intake.

A range of tests are conducted to induce changes to the flow acceleration. This is achieved by modifying the fan location and the beam height, as shown in Figure 1. Two series of studies are performed: 1) The fan is placed at axial locations of $6.2H$ and $7.2H$ with the original beam height (Frames d,f); 2) The beam height is reduced to $1/2H$ and $1/4H$ with the original fan location (Frames c,e).

2.2 Numerical Framework

In the present case, the distortion generator is modeled by the Immersed Boundary Method (IBM), which uses force to fix the velocity at the wall to zero. The IBM method was first proposed by Sirovich [36] to solve the linearized initial and boundary problems. He regarded boundary surfaces in flows as a distribution of sources that can be added to the Navier–Stokes equations. The method was later rigorously proved by Peskin [37] and applications of fluid–structure interactions using IBM can be found in the works of Iaccarino [38] and Fadlun [39]. For the rotational fan, a simplified version of IBM, the Immersed Boundary Method with Smeared Geometry (IBMSG), can be applied. This assumes an infinite number of blades in a row. Hence, the forces in the blade region are circumferentially averaged at every cell and no individual blade passage is resolved. The method was used by Marble [40] to achieve flow turning effects. The application of this method for turbomachines can be found in the work of Cao et al. [11]. They studied intake separation at high incidence and demonstrated that the model is capable of capturing the key flow features. According to the model used by these

authors, the force normal to the blade surface is controlled by the PI controller, which is,

$$f_n(\mathbf{x}, t) = \alpha \int_0^t \Delta u_n dt + \beta \Delta u_n, \quad (1)$$

$$\Delta u_n = u_n(\mathbf{x}_0, t) - u_{n,0}(\mathbf{x}_0, t).$$

The subscript n represents the normal direction and 0 represents the solid boundary. The coefficients α and β are negative constants. Peskin [37] demonstrated that the flow solution is independent of the two coefficients α and β , once convergence has been achieved. Essentially, this force model can be regarded as a proportional-integral (PI) feedback controller. The difference between the actual velocity and the desired velocity $\Delta \mathbf{u}$ contributes to the force and hence controls the flow velocity as equal to the solid velocity \mathbf{u}_0 .

The loss effect can be modeled by a viscous body force, as was assessed and applied by Xu [41] for the unsteady simulation of the distortion transfer through blade passages of a high pressure turbine. Watson [42] developed the model and proposed a typical force–velocity relation,

$$\mathbf{f}_p = -k(4s^2 + 1)\rho \mathbf{u}_{rel}^2, \quad (2)$$

where s is the fraction of span. The force is proportional to $\rho \mathbf{u}_{rel}^2$ and the coefficient k is calibrated using the performance data at the design point from experiments [10]. Further details regarding the implementation of this relation in the compressible Navier–Stokes equations, as well as details concerning blockage models, can be found in [28]. However, it should be noted that this governing equation does not include the turbulence model equations. Hence, for the IBM region, the model is not applicable for the case with a turbulence model or a subgrid-scale model that depends on distance from the wall. To tackle this problem, one may either use wall-resolved boundaries or identify the wall distances and set the relevant turbulence variables, e.g., $k = 0$, $\nu_t = 0$.

3 Validation

3.1 Mixed-fidelity method

The LES-IBMSG method has been validated by Ma et al. [28] in terms of main flow variables and turbulence statistics. Here, the focus is on the RANS-IBMSG method. It is validated on the Darmstadt Transonic Rotor [7–9] using RANS with SA model, as shown in Figure 2. The data for validation are extracted at three cross-sections at $S_1 = 3.5H$, $S_2 = 8.5H$ and $S_3 = 12H$ and the key parameters of this rotor are given in Table 1. The rotor runs at a peak efficiency point (10.6kg/s) with 65% rotational speed (1361.31rad/s). Figure 3 compares the performance map from the numerical simulation with the experiment data from Wartzek [10]. The result shows that this mixed-fidelity method can characterize the general trend of the pressure ratio for the cases with a smooth casing and the distortion generator.

The total pressure distribution downstream of the rotor and stator are shown in Figure 4 (b) and (c) to validate the response of the modeled rotor. The passage data from Wartzek’s experiment [10] and the instantaneous flow from the URANS simulation are also superimposed. The distributions are obtained from the case at the peak efficiency point (10.6kg/s), and extracted at three axial locations ($S_1 \sim S_3$); these are the rotor entry, rotor exit and stator exit respectively. These quantities are defined by,

$$\pi_t = \frac{p_t}{p_{t,inlet}}, \pi_{t,rel} = \frac{\pi_t}{\pi_t} \quad (3)$$

Figure 4 shows these results with the vertical dash lines highlighting the beam installation region. It can be seen that, within this region, the relative total pressure ratio increases from the rotor inlet to the stator outlet (Frames (a) to (c)). This indicates that the distortion recovers downstream but is nonetheless still evident at the outlet. At the rotor and stator outlet, the RANS with IBMSG model is also able to capture the trend. As expected, the variation of the total pressure at each blade region cannot be captured because the blade geometry is smeared but even so, the distribution still shows the asymmetry of the entry and exit, consistent with the resolved case and experiment. To validate how the mixed-fidelity simulation characterizes

the separation, the mass flux distribution is compared with the mesh-resolved case in Figure 5. The mass flux is obtained at the axial location $x = 4.5H$ in front of the fan. Evidently, the momentum deficit occurs at $y = 0$ to $1.5H$, within the beam height. The result from the modeled case shows a good agreement with the resolved case.

The validation indicates that, although the separation affects the flow in both the rotor and stator regions, the mixed-fidelity method can still accurately capture the main flow features between the fan and the distortion generator. This also means that separated flows do not have any obvious impact on the performance by this method.

3.2 Mesh independence

A range of fan–intake interaction studies are undertaken using LES. Since LES results highly depend on the mesh resolution, a mesh independence study is performed before any detailed flow physics analysis takes place. Two mesh resolutions are tested and the number of nodes for the coarse and fine meshes are 8.6 million and 60 million, respectively. The fine mesh is examined using criteria related to the Kolmogorov length scale; details can be found in [28]. The dimensionless spacing constraints for the two meshes in each of the three directions can be found in Table 2. Figure 7 compares the axial velocity and TKE at the position $x = 4.5H$ predicted on the coarse and fine meshes. It can be seen that neither distribution is visibly influenced by the mesh size, thus indicating that mesh independence has been achieved.

4 RANS versus LES

In this section, the data collected from the RANS and time-averaged LES models are discussed. Note that the RANS simulations are also carried out on the LES mesh comprising of 8.6M nodes, for which mesh independence has been shown in Figure 7. The averaging process starts when a fully developed flow is achieved and lasts for approximately 15 flowthrough times. These comparative studies contain distorted flows 1) without a fan, 2) with a fan at different axial locations and 3) with different beam heights and a fan fixed at the original location (see Fig.1). To investigate how these factors influence the prediction of the separated flows, we focus on the profiles of the velocity and the TKE, non-dimensionalized by u_∞ and

u_∞^2 , respectively. The reference velocity u_∞ is measured in the main flow near the edge of the beam.

To quantify the effect of the fan and the discrepancies between the RANS and LES approaches, we use two non-dimensionalized parameters; the acceleration parameter, K , and the discrepancy in the angle of the blade incidence, $\Delta\theta$. The former is defined according to Launder [43], as

$$K = \frac{v}{u_\infty^2} \frac{\partial U}{\partial x}. \quad (4)$$

The discrepancy between the RANS and LES model results can be critical in terms of predicting the downstream fan performance, so we relate it to the incidence angles and define

$$\theta = \tan^{-1} \frac{r\Omega}{U} - \theta_b, \Delta\theta = \theta_{RANS} - \theta_{LES}, \quad (5)$$

where θ_b is the blade leading-edge angle.

4.1 Distortion without fan

Figure 6 illustrates the velocity and TKE profiles for distorted flows in the contracting duct without a fan. Evidently, the discrepancies are significant within the separation region for both the $k-\omega$ and SA models in the region near the casing. Frame (b) shows that the TKE predicted by the RANS ($k-\omega$) model is considerably higher than that predicted by LES. The overestimated TKE equates to stronger turbulence, and thus leads to a stronger mixing process. As a result, the distorted flow has reattached at $x = 5H$ in RANS case, which is much earlier than the result from the LES.

This discrepancy can be explained from the turbulence equations of the $k-\omega$ model, which

are

$$\begin{aligned}\frac{\partial(\rho k)}{\partial t} + \frac{\partial(\rho u_j k)}{\partial x_j} &= \mathcal{P} - \mathcal{D}(k, \omega) + \mathcal{F}(k, \omega) \\ \frac{\partial(\rho \omega)}{\partial t} + \frac{\partial(\rho u_j \omega)}{\partial x_j} &= \frac{\gamma \omega}{k} \mathcal{P} - \mathcal{D}(k, \omega) + \mathcal{F}(k, \omega).\end{aligned}\tag{6}$$

These indicate that the difference may come from the production term $\mathcal{P} = -\rho u'_i u'_j \frac{\partial U_i}{\partial x_j}$. As a eddy viscosity model, it assumes that Reynolds stresses are proportional to the strain tensor.

$$\begin{aligned}-\rho u'_i u'_j &= 2\nu_t S_{ij} - \frac{2}{3}k\delta_{ij}, \\ S_{ij} &= \frac{1}{2} \left(\frac{\partial U_i}{\partial x_j} + \frac{\partial U_j}{\partial x_i} \right), \\ \nu_t &= \rho k / \omega\end{aligned}\tag{7}$$

Hence, the problem could either be associated with this linear relation between the stresses and strains or from the incorrect strain tensor S_{ij} field. To clarify this point, we fix the velocities according to LES results and repeat the case with the $k - \omega$ model. This strategy is similar to that of Gao and Liu et al. [44]. Figure 8 reveals that, even if the strain tensor is the same as the LES case, the TKE values are still differ significantly; the RANS result is almost three times larger than the LES value. This is because the velocity gradient $\frac{\partial U}{\partial y}$ is the dominant term in the TKE production within the reversed flow and its value is higher in the RANS case compared to the LES model. Accordingly, the production of TKE in the RANS with velocities fixed by those in the LES also increases. This increase is approximately quadratic since $\mathcal{P}_{12} = \nu_t \left(\frac{\partial U}{\partial y} \right)^2$.

Hence, we may conclude that this linear relation is not applicable for this separated flow. According to Craft et al. [32], the result can be improved by adding a quadratic term to Equation 7, which term is aimed at reducing the production. On the other hand, turbulence models are constructed based on the local equilibrium between turbulence production and destruction; however, this equilibrium state could be destroyed and strong non-equilibrium turbulence could then dominate when separation occurs [21]. Based on this concept, Liu et al. [15] made

a first attempt to modify a turbulence model using helicity in order to take account of the turbulence energy backscatter when considering turbulence non-equilibrium in vortical flows. They modified the SA model using helicity, and the results showed that the modified SA model was able to significantly improve the predictive accuracy when simulating corner separation flow in compressors [45]. Recently, the modified SA model was also successfully used to predict the behavior of fan flows at off-design conditions [46].

Therefore, for the case without a fan, the turbulence model is important and may substantially affect the prediction. Hence, an eddy resolving simulation is preferred.

4.2 Distortion with Fan effect

This section discusses the influence of a fan on the characteristics of the distortion. Figure 9 shows the influence of the fan on the flow without any distortion, as characterized by the mass flux. Evidently, the fan is able to accelerate the flow near the casing and decelerate it near the hub. When the beam is installed at the casing, this acceleration has a significant impact in reducing the bubble. The line in Figure 10 connects the inflectional points of the velocity profile at different streamwise locations and circles the separation region, which denotes the bubble size. It is noticeable that the fan reduces the recirculation region by a length scale that is greater than the beam height.

4.2.1 Effects of fan location

The effect of fan can be modified by placing it at different locations. The original fan is installed at $x = 5.2H$. Then, it is moved downstream to two locations: ‘Loc1’, a distance of a half-chord ($x = 6.2H$) and ‘Loc2’, a full chord distance ($x = 7.2H$).

Figure 11 shows the change in the velocity profiles when the fan is placed at different locations. It is clear that, when the fan is installed, it significantly accelerates the flow and changes the streamline curvature. When the fan is at the original location, the difference between RANS and LES is almost eliminated. In Frame (a), the velocity profiles almost overlap near the leading edge of the fan (at $x = 5H$). This applies to both the $k - \omega$ model and the SA model. As the fan effect becomes weaker due to the increased distance (Frame (b) and (c)), the difference between the RANS and LES profiles becomes larger. In this situation, a high-

fidelity simulation, which resolves turbulence, is more reliable.

To investigate how the discrepancy in the velocity profiles impacts the flow at the fan face, we extract the total pressure distribution, acceleration parameter and angle of incidence at $x = 4.5H$, as shown in Figure 12. Frame (a) shows that the original location has the highest effect in terms of increasing the total pressure ratio, whereas the fan placed further away (illustrated by the blue curves for $x = 6.2H$ and black curves for $x = 7.2H$) had less of an influence in suppressing the distortion. There is also an increasing trend in the discrepancy between the RANS and LES models when fan is moved towards downstream. When the fan is placed at Location 0, both the RANS and LES models successfully predict almost the same the total pressure. This means that resolving of the turbulence may not be necessary and the RANS approach might be sufficient. When the fan is placed at the other locations, or in the case without fan, however, the rising discrepancies indicate that the RANS results may be unreliable near the casing.

Frame (b) compares the acceleration parameter, K , extracted at the same location. The flow for the case 'Loc0' has reattached whereas it remains separated in the other cases. Evidently, the fan at the original location induces the highest acceleration (the line for 'Loc0, H'), followed by the cases in which the fan is at Locations 1 and 2, meaning that the further away the location of the fan is, the weaker acceleration.

Frame (c) shows the angle of incidence at this fan face from the LES with the 'error bands from RANS. The case without a fan represents the most significant difference. In contrast, the case 'Loc0, H' has the lowest discrepancy due to the downstream fan effect. When the fan is moved downstream to Locations 1 or 2, the discrepancies become larger. This indicates that the prediction of the separated flow under high acceleration depends less on the RANS model.

4.2.2 Effects of beam height

The effect of the fan in terms of the different distortions induced is also investigated using two beams with difference heights, $1/2H$ and $1/4H$, installed at the same location. Figure 13 plots the velocity profiles from both the RANS and LES results.

It should be noted that the distorted flows reattach at difference axial locations, which are

much earlier for the case with the smaller beam. Due to the difference in the separation regions, the data cannot be compared at the same actual location. For consistency, we focus on the data outside of the separation region, i.e., in the boundary layer after reattachment $x > 4H$. As expected, although the region of the discrepancy may be reduced further away from the casing, its maximum near the wall increases.

The discrepancies in regard to the velocity near the wall have an influence on the total pressure upstream of the fan, as shown in Frame (a) of Figure 14. Near the wall, the difference between the RANS and LES models increases when the beam height is reduced and the acceleration is weakened. Hence, for these cases, turbulence or the wall effect plays a more important role, so an eddy-resolving method is essential.

To characterize the fans influence on the different inflow distortions, the acceleration parameter K is plotted in Frame (b), extracted at $x = 4.5H$. The $1/2H$ beam generates a higher acceleration than the $1/4H$ beam with the same fan. This is reasonable because, for a larger obstacle, the streamline curvature is larger, and thus the acceleration is stronger. The corresponding discrepancies in the predicted incidence angles are depicted in Frame (c). Evidently, as the acceleration is reduced, the incidence angle decreases, as does its discrepancy near the wall, $y = 0$. Hence, the wall effect surpasses the main flow as a more significant influence and thus the eddy-resolving method is necessary when predicting boundary layers around blade tips in this scenario.

4.3 Acceleration and discrepancies between RANS and LES

All of the previous cases show a trend such that, if the acceleration parameter is higher, the turbulence is less influential on the separation prediction. It should be noted that the maximums of the two parameters K and $\Delta\theta$ are usually around the casing, hence they may severely affect fan performance at the tip and change the tip leakage flows significantly. Figure 15 plots the maximum of the discrepancy in $\Delta\theta$ at the casing with increasing acceleration parameter for all the test cases with varying fan-locations and beam-heights.

The black line with square symbols connects the results for the fan installed at different locations. It shows that the flow acceleration can significantly reduce the error associated

with the RANS approach. For the case with the original fan location, a strong acceleration is observed. The difference between the RANS and LES is marginal. The extreme case is such that the substantial flow acceleration can lead to the same predictions between the RANS and LES models. Hence, when close to this situation, the RANS model may be sufficient for separation prediction. The red line with circular symbols denotes the difference in the incidence angles on the casing for the cases with different beams. Similarly, the discrepancies decrease when the flow acceleration is stronger.

The reduction of the discrepancies between the RANS and LES models also indicates that, with sufficient acceleration, the main flow can significantly affect the turbulence, whereas the turbulence effect on the prediction is very limited. Figure 16 shows that when the fan is installed at the original location, it dominates the main flow and the TKE profiles are very similar, despite a slight deviation in the distributions.

The effect of turbulence can be further examined by comparing a case with a lower Reynolds number. The flow for the present case is at $Re = 1 \times 10^6$ and the relevant references are the inlet velocity and duct radius. An additional case is defined by increasing the viscosity by an order of magnitude, and thus $Re = 1 \times 10^5$. The same fan is installed. Figure 17 depicts the velocity and TKE profiles for both cases (with higher and lower viscosity). The TKE for the flow with the lower Reynolds number (blue curve) is slightly weaker around the shear layer $y = H$ and near the wall. Although this weakened turbulence changes the velocity profile at $x = H$ and near the wall, it does not affect any other area. Hence, this explicitly demonstrates that the turbulence does not have a strong impact on the forced separated flow.

5 Conclusions

The current paper intends to investigate the discrepancies between RANS and LES in the presence of a downstream fan. More specifically, the downstream fan effects the mass flow redistribution and accelerates the flow at the casing relative to the hub. The present paper investigates the consequence of this acceleration on the RANS-LES discrepancies using a mixed fidelity method.

A beam-shaped distortion generator is modeled using the IBM; the rotational fan is ap-

proximated by the IBMSG approach. The numerical framework is validated using a transonic rotor by comparing it to the mesh-resolved case and experiments. Thorough comparisons indicate that the mixed-fidelity method is accurate enough to predict the general trends in the performance map and the total pressure distributions at the rotor inlet, exit and stator exit.

Subsequently, the mixed-fidelity method is deployed to investigate a range of cases with various flow accelerations. This is achieved by installing a fan downstream of the distortion generator and varying its proximity to the distortion generator. Test cases for a given fan-location and varying heights of the distortion generator are also investigated.

In the "absence of fan", the discrepancies between RANS and LES is significant within the separation and reattachment region, due to the well-known limitations of the standard RANS models. Interestingly, the current study shows that "with the fan installed", the deviation between RANS and LES decreases substantially. Specifically, the deviation is minimal when the proximity of the fan is closest to the separation. It implies that with an installed fan, the inaccuracies of the turbulence model are mitigated by the strong flow acceleration at the casing due to the fan. More precisely, the mass flow redistribution due to the fan has a dominant primary effect on the final predictions and the effect of turbulence model becomes secondary, thereby suggesting that high fidelity eddy resolving simulations like LES provide marginal improvements to the accuracy for the installed cases. These results are particularly important for the short intake-fan strategies with fan getting closer to intake lip.

Acknowledgements

The authors acknowledge the computing time on the UK national high-performance computing service ARCHER provided via the UK Turbulence Consortium in the framework of the EPSRC grant EP/L000261/1. This work is also funded by the studentship from Chinese Scholarship Council. The code for this project is provided by the Rolls-Royce plc. All the funding and technical support from these organizations are gratefully acknowledged.

Funding

The Engineering and Physical Sciences Research Council (EPSRC) grant EP/L000261/1.
The Chinese Scholarship Council (CSC) No. 201506020121.

Nomenclature

f force

H height of the beam

k coefficient for viscosity distribution

k_t turbulence kinetic energy

n normal vector to the blade surface

t time or blade thickness

p pressure

u velocity

x x coordinate

x_0 body/surface coordinate

$u'_i u'_j$ Reynolds stresses

Δy_+ dimensionless wall distance

Δx_+ dimensionless streamwise distance

Δz_+ dimensionless spanwise distance

K flow acceleration parameter

$P_{t,loss}$ mass-weighted total pressure loss

S_{ij} mean rate of strain tensor

U_i main flow velocity

\mathcal{P} production term in $k - \omega$ model

\mathcal{D} destruction term in $k - \omega$ model

\mathcal{F} diffusion term in $k - \omega$ model

α, β feedback forcing coefficients

γ coefficient in $k - \omega$ model

ρ density

ν_t turbulence viscosity

π_t total pressure ratio

θ incidence angle

RANS Reynolds Averaged Navier-Stokes

URANS Unsteady Reynolds Averaged Navier-Stokes

LES Large Eddy Simulation

IBM Immerse Boundary Method

BFM Body Force Method

FSM Fan Similarity Model

IBMSG Immersed Boundary Method with Smeared Geometry

SA Spalart-Allmaras turbulence model

$k - \omega$ $k - \omega$ turbulence model

References

- [1] Longley, J., and Greitzer, E., 1992. "Inlet distortion effects in aircraft propulsion system integration".
- [2] Tucker, P., 2013. *Unsteady computational fluid dynamics in aeronautics*, Vol. 104. Springer Science & Business Media.
- [3] Defoe, J. J., and Spakovszky, Z. S., 2013. "Effects of boundary-layer ingestion on the aero-acoustics of transonic fan rotors". *ASME J. Turbomach.*, **135**(5), p. 051013.
- [4] Fidalgo, V. J., Hall, C., and Colin, Y., 2012. "A study of fan-distortion interaction within the nasa rotor 67 transonic stage". *ASME J. Turbomach.*, **134**(5), p. 051011.
- [5] Barthmes, S., Haug, J. P., Lesser, A., and Niehuis, R., 2016. "Unsteady cfd simulation of transonic axial compressor stages with distorted inflow". In *Advances in Simulation of Wing and Nacelle Stall*. Springer, pp. 303–321.
- [6] Xie, Z., Liu, Y., Liu, X., Sun, D., Lu, L., and Sun, X., 2017. "Computational model for stall inception and nonlinear evolution in axial flow compressors". *Journal of Propulsion and Power*, pp. 1–10.
- [7] Lieser, J., Biela, C., Pixberg, C., Schiffer, H.-P., Schulze, S., Lesser, A., Kähler, C., and R, N., 2011. "Compressor rig test with distorted inflow using distortion generators".
- [8] Niehuis, R., Lesser, A., Probst, A., Radespiel, R., Schulze, S., Kähler, C., Spiering, F., and Kroll, N., 2013. "Simulation of nacelle stall and engine response".
- [9] Übelacker, S., Hain, R., and Kähler, C. J., 2016. "Flow investigations in a stalling nacelle inlet under disturbed inflow". In *Advances in Simulation of Wing and Nacelle Stall*. Springer, pp. 271–283.
- [10] Wartzek, F., Holzinger, F., Brandstetter, C., and Schiffer, H.-P., 2016. "Realistic inlet distortion patterns interacting with a transonic compressor stage". In *Advances in Simulation of Wing and Nacelle Stall*. Springer, pp. 285–302.
- [11] Cao, T., Hield, P., and Tucker, P. G., 2017. "Hierarchical immersed boundary method with smeared geometry". *Journal of Propulsion and Power*, pp. 1–13.
- [12] Carnevale, M., Wang, F., Parry, A. B., Green, J. S., and di Mare, L., 2018. "Fan similarity model for the fan–intake interaction problem". *Journal of Engineering for Gas Turbines*

and Power, **140**(5), p. 051202.

- [13] Liu, Y., Yu, X., and Liu, B., 2008. “Turbulence models assessment for large-scale tip vortices in an axial compressor rotor”. *Journal of Propulsion and Power*, **24**(1), pp. 15–25.
- [14] Liu, Y., Yan, H., Liu, Y., Lu, L., and Li, Q., 2016. “Numerical study of corner separation in a linear compressor cascade using various turbulence models”. *Chinese Journal of Aeronautics*, **29**(3), pp. 639–652.
- [15] Liu, Y., Lu, L., Fang, L., and Gao, F., 2011. “Modification of spalart–allmaras model with consideration of turbulence energy backscatter using velocity helicity”. *Physics Letters A*, **375**(24), pp. 2377–2381.
- [16] Scillitoe, A. D., Tucker, P. G., and Adami, P., 2015. “Evaluation of rans and zdes methods for the prediction of three-dimensional separation in axial flow compressors”. In ASME Turbo Expo 2015: Turbine Technical Conference and Exposition, American Society of Mechanical Engineers, pp. V02BT39A041–V02BT39A041.
- [17] Tyacke, J., Tucker, P., Jefferson-Loveday, R., Vadlamani, N. R., Watson, R., Naqavi, I., and Yang, X., 2014. “Large eddy simulation for turbines: methodologies, cost and future outlooks”. *ASME J. Turbomach.*, **136**(6), p. 061009.
- [18] Tucker, P., and Liu, Y., 2006. “Turbulence modeling for flows around convex features”. In 44th AIAA Aerospace Sciences Meeting and Exhibit, p. 716.
- [19] Liu, Y., Yan, H., Lu, L., and Li, Q., 2017. “Investigation of vortical structures and turbulence characteristics in corner separation in a linear compressor cascade using ddes”. *ASME J. Fluids Eng.*, **139**(2), p. 021107.
- [20] Scillitoe, A. D., Tucker, P. G., and Adami, P., 2017. “Numerical investigation of three-dimensional separation in an axial flow compressor: The influence of freestream turbulence intensity and endwall boundary layer state”. *ASME J. Turbomach.*, **139**(2), p. 021011.
- [21] Yan, H., Liu, Y., Li, Q., and Lu, L., 2018. “Turbulence characteristics in corner separation in a highly loaded linear compressor cascade”. *Aerospace Science and Technology*, **75**, pp. 139–154.
- [22] Gourdain, N., Gicquel, L. Y., and Collado, E., 2012. “Comparison of rans and les for

prediction of wall heat transfer in a highly loaded turbine guide vane”. *Journal of propulsion and power*, **28**(2), pp. 423–433.

- [23] Thollet, W., Dufour, G., Carbonneau, X., and Blanc, F., 2016. “Assessment of body force methodologies for the analysis of intake-fan aerodynamic interactions”. In ASME Turbo Expo 2016: Turbomachinery Technical Conference and Exposition, American Society of Mechanical Engineers, pp. V02CT39A036–V02CT39A036.
- [24] Damle, S. V., Dang, T. Q., and Reddy, D. R., 1995. “Throughflow method for turbomachines applicable for all flow regimes”. *ASME J. Turbomach.*, **119**(2), p. V001T01A098.
- [25] Sturmayer, A., and Hirsch, C., 1999. “Throughflow model for design and analysis integrated in a three-dimensional navier-stokes solver”. *Proceedings of the Institution of Mechanical Engineers Part A Journal of Power & Energy*, **213**(4), pp. 263–273.
- [26] Simon, J. F., and Leonard, O., 2005. “A throughflow analysis tool based on the navier-stokes equations”. In 6th European Conference on Turbomachinery Fluid Dynamics and Thermodynamics.
- [27] Persico, G., and Rebay, S., 2012. “A penalty formulation for the throughflow modeling of turbomachinery”. *Computers & Fluids*, **60**(10), pp. 86–98.
- [28] Ma, Y., Cui, J., Vadlamani, N. R., and Tucker, P. “Effect of fan on inlet distortion: A mixed-fidelity approach”. *AIAA J.*
- [29] Ma, Y., Cui, J., Vadlamani, N. R., and Tucker, P., 2018. “A mixed-fidelity numerical study for fan-distortion interaction”. In ASME Turbo Expo 2018: Turbine Technical Conference and Exposition, American Society of Mechanical Engineers, pp. V003T06A022–V003T06A022.
- [30] Scillitoe, A. D., Tucker, P. G., and Adami, P., 2015. “Evaluation of rans and zdes methods for the prediction of three-dimensional separation in axial flow compressors”. In ASME Turbo Expo 2015: Turbine Technical Conference and Exposition, American Society of Mechanical Engineers, pp. V02BT39A041–V02BT39A041.
- [31] Iaccarino, G., Mishra, A. A., and Ghili, S., 2017. “Eigenspace perturbations for uncertainty estimation of single-point turbulence closures”. *Physical Review Fluids*, **2**(2), p. 024605.
- [32] Craft, T., Launder, B., and Suga, K., 1997. “Prediction of turbulent transitional phenomena

- with a nonlinear eddy-viscosity model”. *International Journal of Heat and Fluid Flow*, **18**(1), pp. 15–28.
- [33] Tucker, P. G., 2016. *Advanced computational fluid and aerodynamics*, Vol. 54. Cambridge University Press.
- [34] Reid, C., 1969. “The response of axial flow compressors to intake flow distortion”. In ASME 1969 Gas Turbine Conference and Products Show, American Society of Mechanical Engineers, pp. V001T01A029–V001T01A029.
- [35] Haug, J., Barthmes, S., and Niehuis, R., 2015. “Full annulus unsteady cfd simulations on effects of inflow distortions in a transonic axial compressor stage”. In Proceedings of 11th International Gas Turbine Congress, no. IGTC-2015-090.
- [36] Sirovich, L., 1967. “Initial and boundary value problems in dissipative gas dynamics”. *The Physics of Fluids*, **10**(1), pp. 24–34.
- [37] Peskin, C. S., 2002. “The immersed boundary method”. *Acta numerica*, **11**, pp. 479–517.
- [38] Iaccarino, G., and Verzicco, R., 2003. “Immersed boundary technique for turbulent flow simulations”. *Applied Mechanics Reviews*, **56**(3), pp. 331–347.
- [39] Fadlun, E., Verzicco, R., Orlandi, P., and Mohd-Yusof, J., 2000. “Combined immersed-boundary finite-difference methods for three-dimensional complex flow simulations”. *Journal of computational physics*, **161**(1), pp. 35–60.
- [40] Marble, F. E., 1964. “Three-dimensional flow in turbomachines”. *High Speed Aerodynamics and Jet Propulsion*, **10**, pp. 83–166.
- [41] Xu, L., 2002. “Assessing viscous body forces for unsteady calculations”. In ASME Turbo Expo 2002: Power for Land, Sea, and Air, American Society of Mechanical Engineers, pp. 323–331.
- [42] Watson, R., Cui, J., Ma, Y., and Hield, P., 2017. “Improved hierarchical modelling for aerodynamically coupled systems”. In ASME Turbo Expo 2017: Turbine Technical Conference and Exposition, American Society of Mechanical Engineers.
- [43] Launder, B. E., and Jones, W. P., 1969. *On the prediction of laminarisation*. HM Stationery Office.
- [44] Gao, Y., Liu, Y., Zhong, L., Hou, J., and Lu, L., 2016. “Study of the standard k- ϵ model

for tip leakage flow in an axial compressor rotor”. *International Journal of Turbo & Jet-Engines*, **33**(4), pp. 353–360.

[45] Tang, Y., Liu, Y., and Lu, L., 2018. “Solidity effect on corner separation and its control in a high-speed low aspect ratio compressor cascade”. *International Journal of Mechanical Sciences*, **142**, pp. 304–321.

[46] Kim, S., Pullan, G., and Hall, C., 2018. “Stall inception in low pressure ratio fans”. In ASME Turbo Expo 2018: Turbine Technical Conference and Exposition, No. GT2018-75153, American Society of Mechanical Engineers.

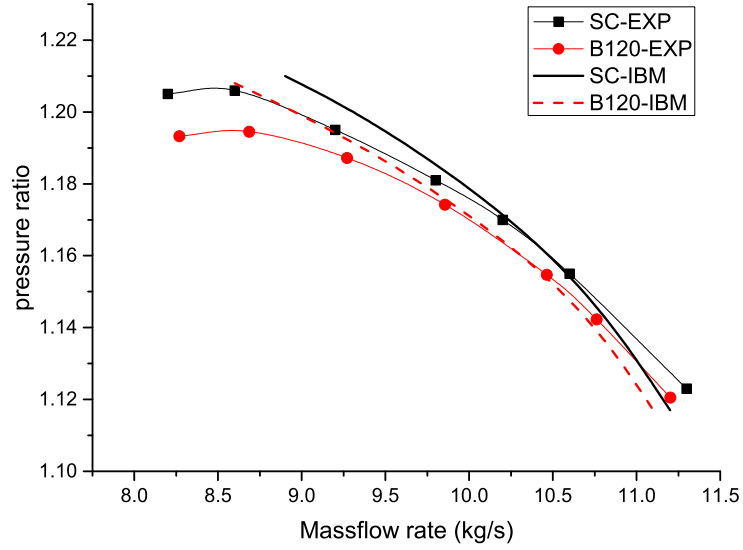


Fig. 3: Performance map of the Darmstadt Rotor at 65% Rotating Speed (SC: Smooth Casing, B120: 120° beam)

Table 2: Grid spacing in the region between the beam and fan

Grid size	Δx^+	Δy^+	Δz^+	Number of nodes
Coarse grid	150	1	100	8,600,100
Fine grid	75	1	30	59,371,200

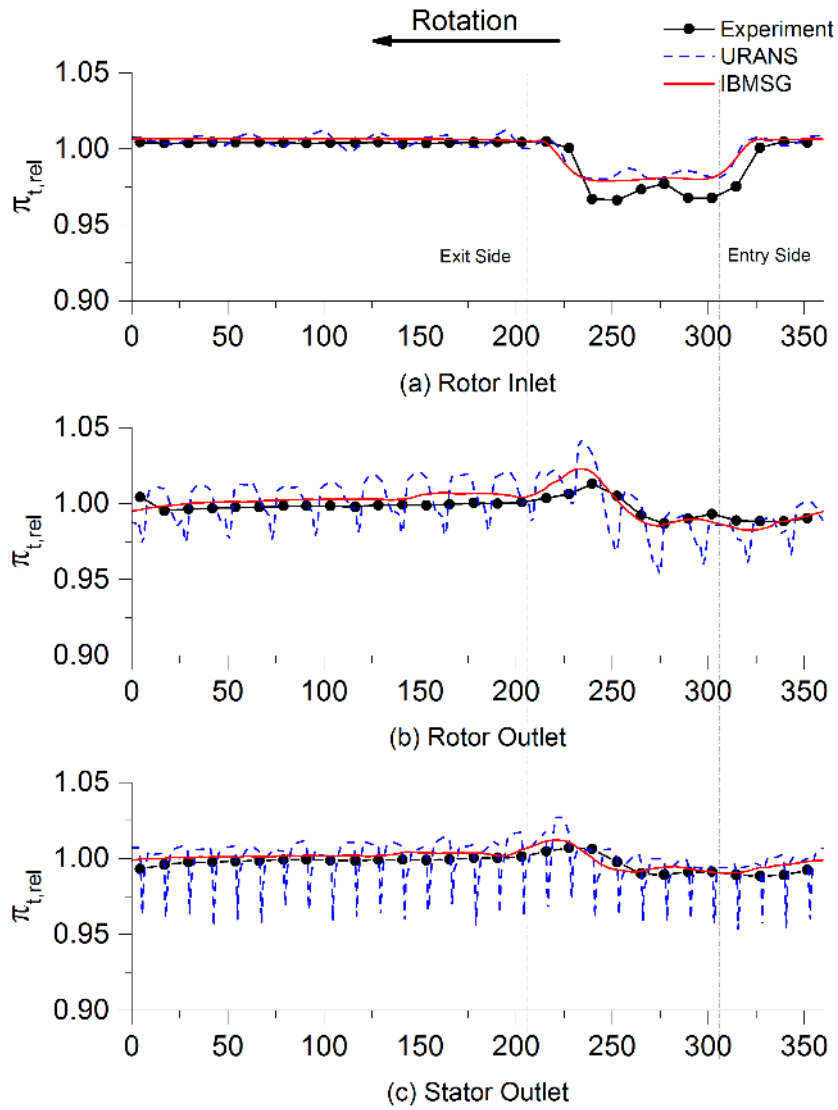


Fig. 4: Circumferential variation of total pressure distribution for 65% speed, monitored at (a) rotor inlet (b) rotor outlet (c) stator outlet

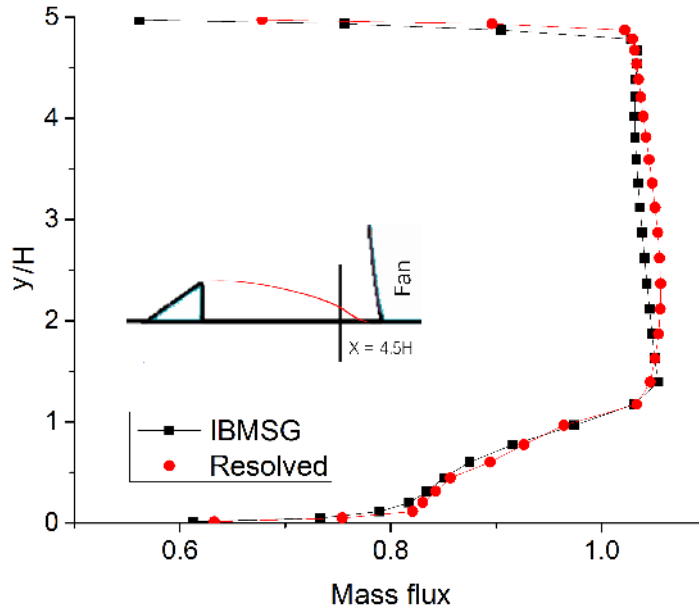


Fig. 5: Radial variation of mass flux at $x = 4.5H$, using IBMSG and geometry resolved approach. Fan placed at Location 0

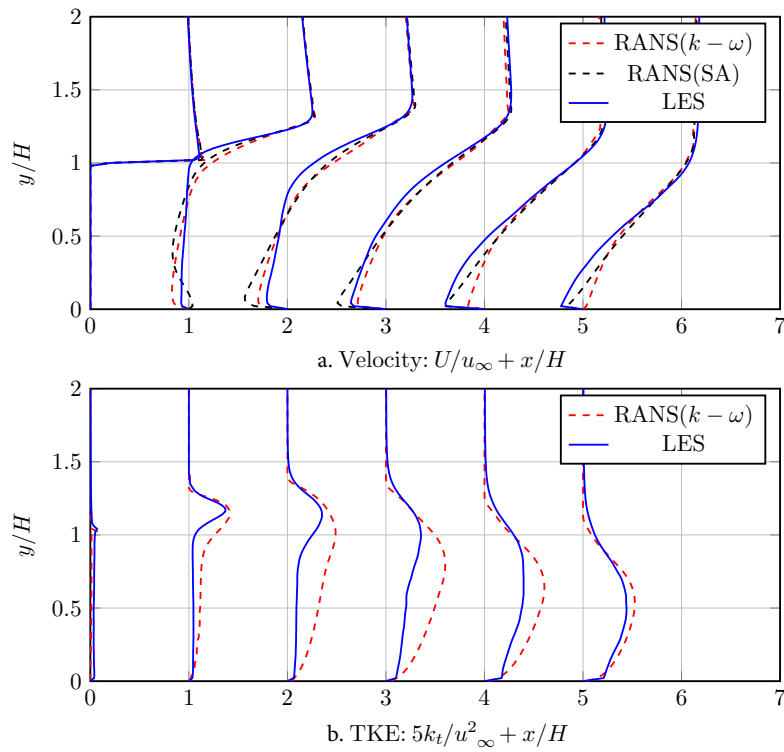


Fig. 6: Carpet plots comparing the (a) Velocity profiles and (b) TKE profiles between RANS and LES for the case Duct, H (without fan)

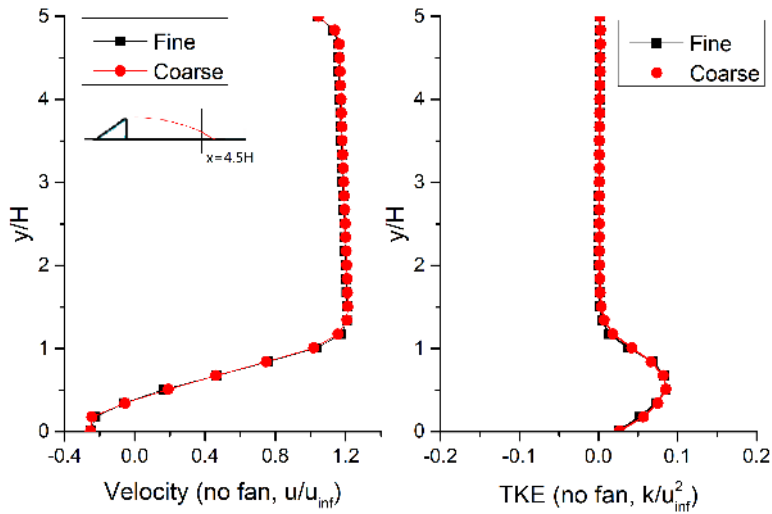


Fig. 7: Mesh sensitivity study from LES showing the radial variation of (a) velocity and (b) TKE at $x = 4.5H$, for the case Duct H without fan

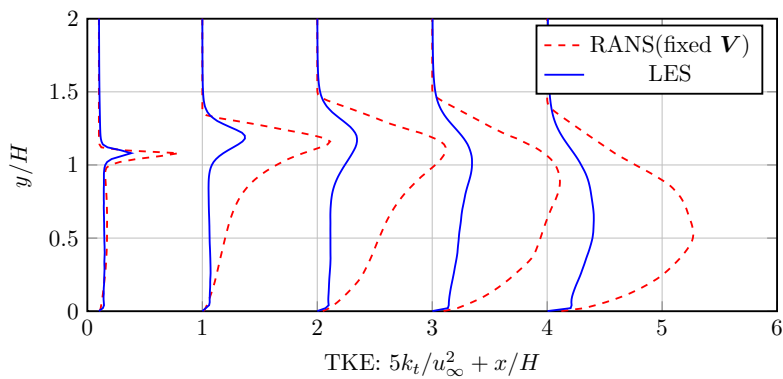


Fig. 8: Comparison of TKE profiles obtained from LES against the RANS (with frozen velocity field from LES), for the case Duct H without fan

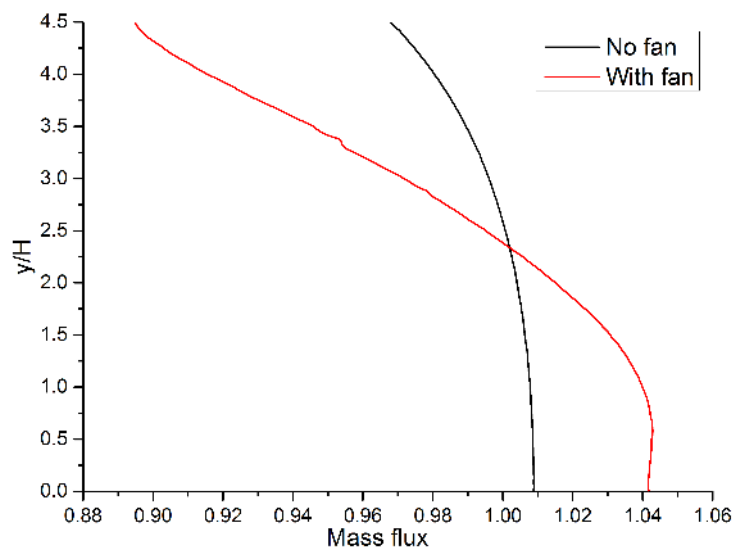


Fig. 9: Radial variation of mass flux with and without fan

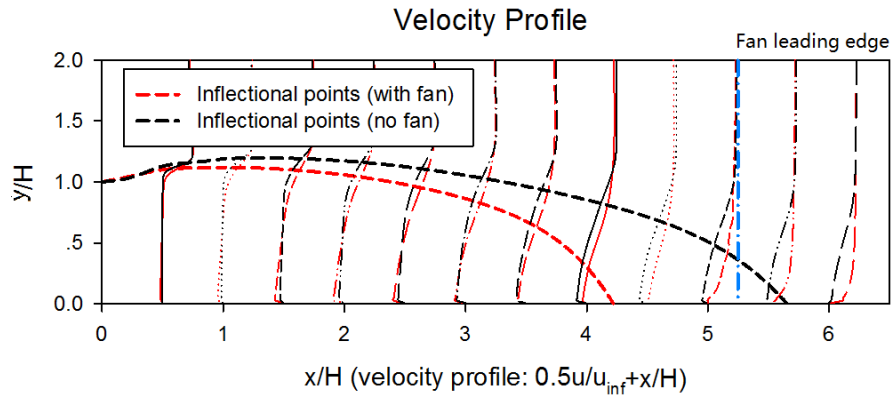


Fig. 10: Carpet plot showing the velocity profiles with and without fan. Locus of inflectional points are also overlaid. Dash-dotted line(blue online) corresponds to fan leading edge location

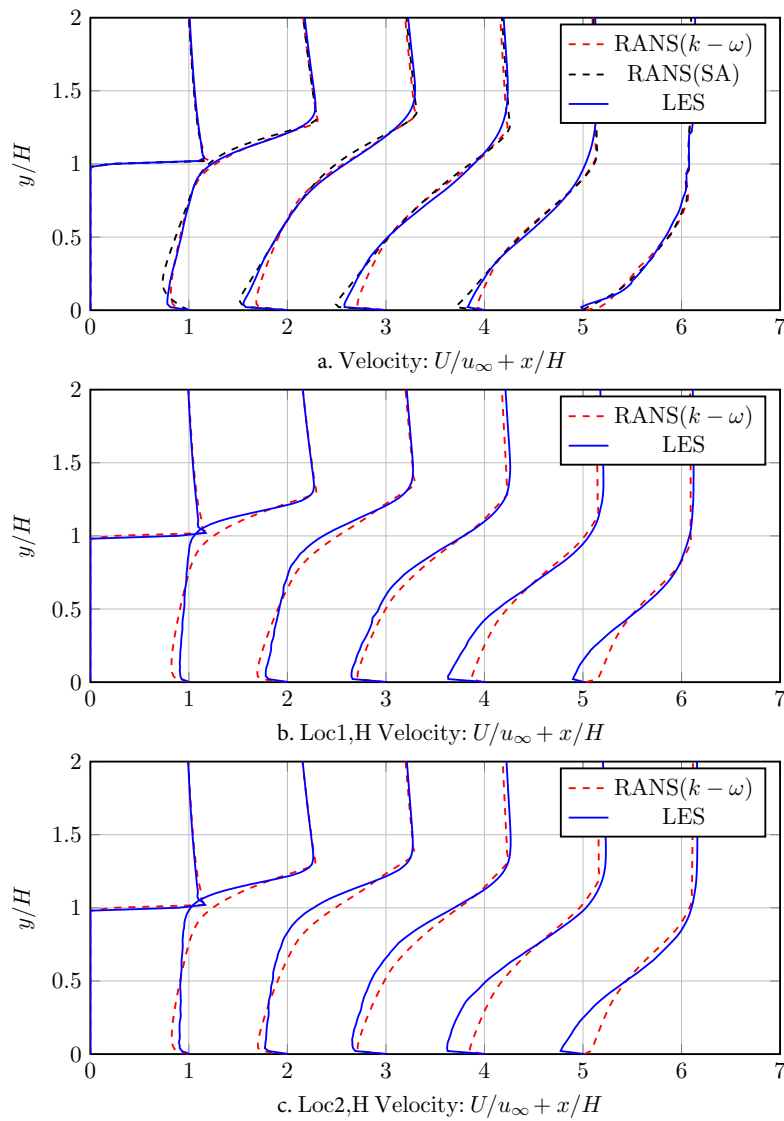
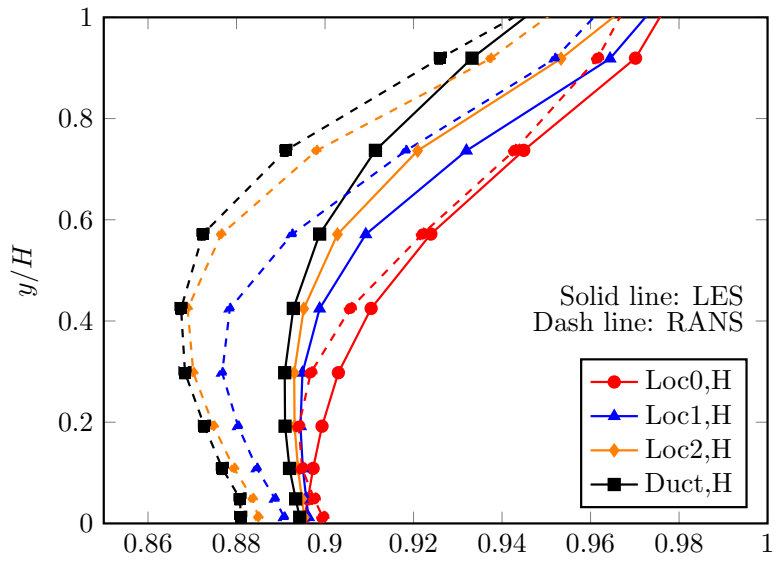
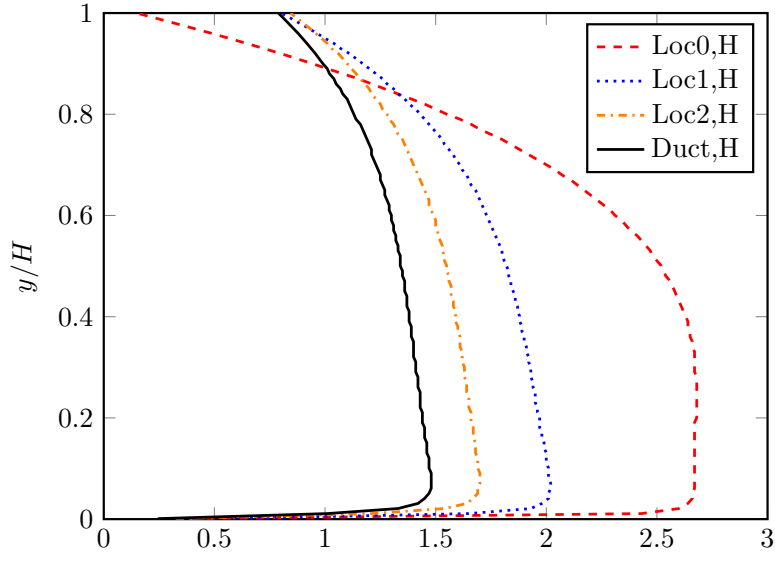


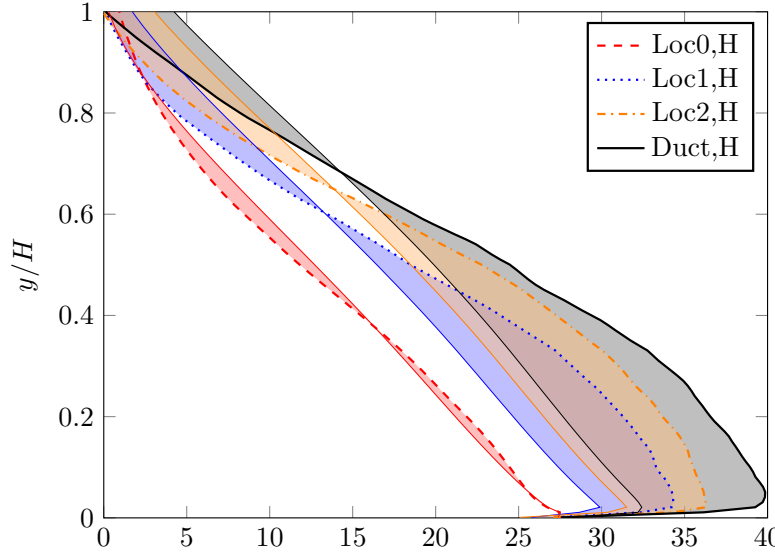
Fig. 11: Carpet plots comparing velocity profiles predicted by RANS against LES for a given distortion generator of height, H and varying fan-locations: cases (a) Loc 0 (b) Loc 1 (c) Loc 2



(a). π_t



(b). $K \times 10^{-6}$



(c). θ°

Fig. 12: Radial distributions of (a) total pressure ratio (b) acceleration parameter (c) angle of incidence predicted by RANS and LES at $x = 4.5H$. Cases compared for same beam height, H and varying fan-location: Loc0, Loc1, Loc2. Test case without fan (Duct, H) is also shown.

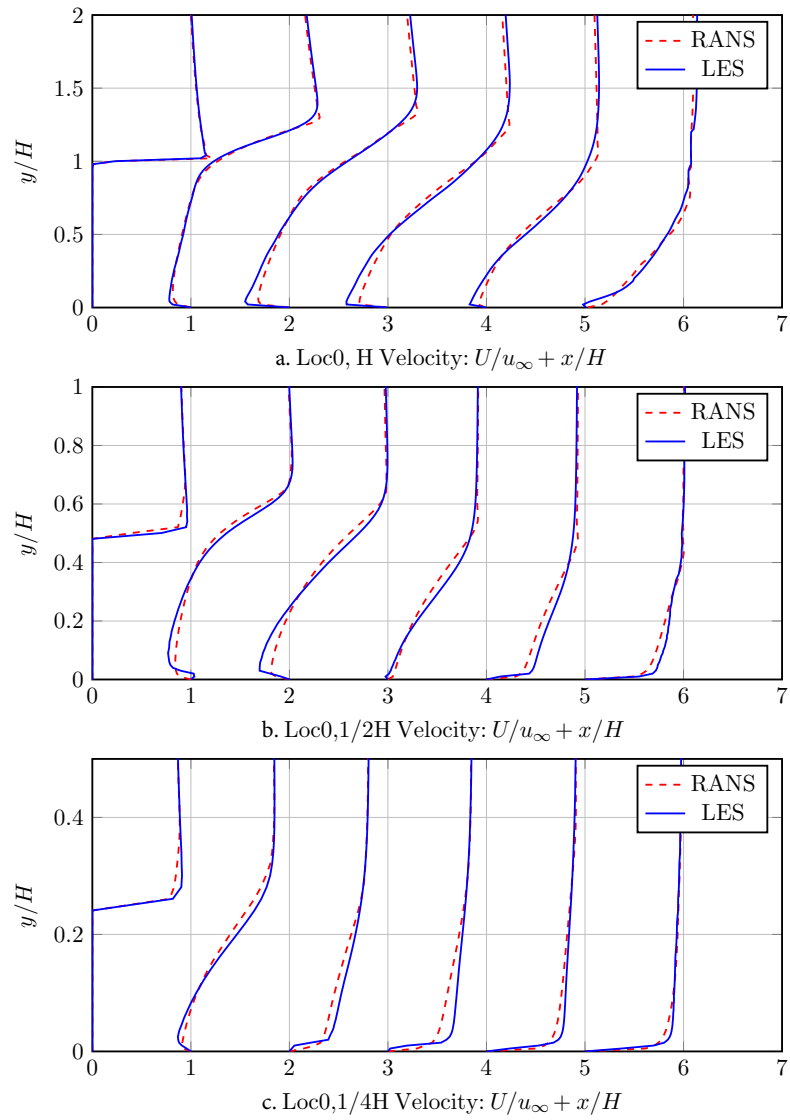


Fig. 13: Carpet plots comparing the velocity profiles predicted by RANS and LES for a given fan-location Loc0 and varying beam heights (a) H (b) H/2 (c) H/4

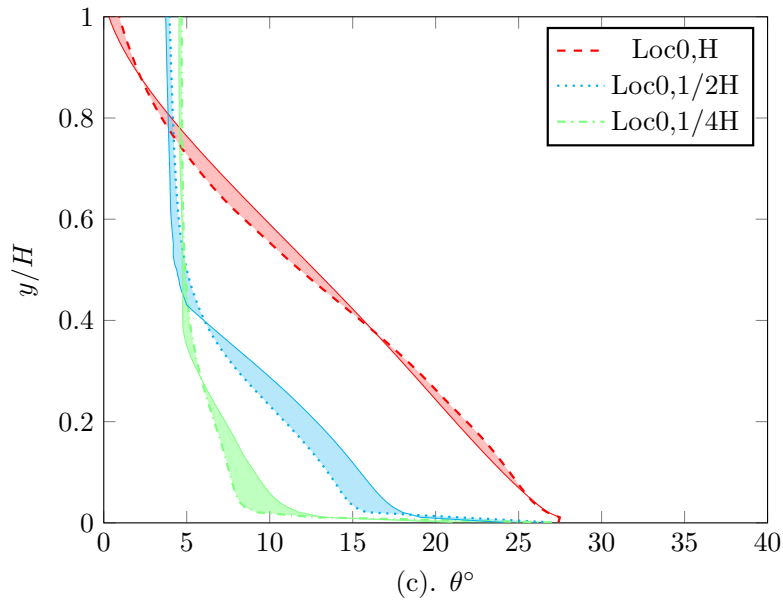
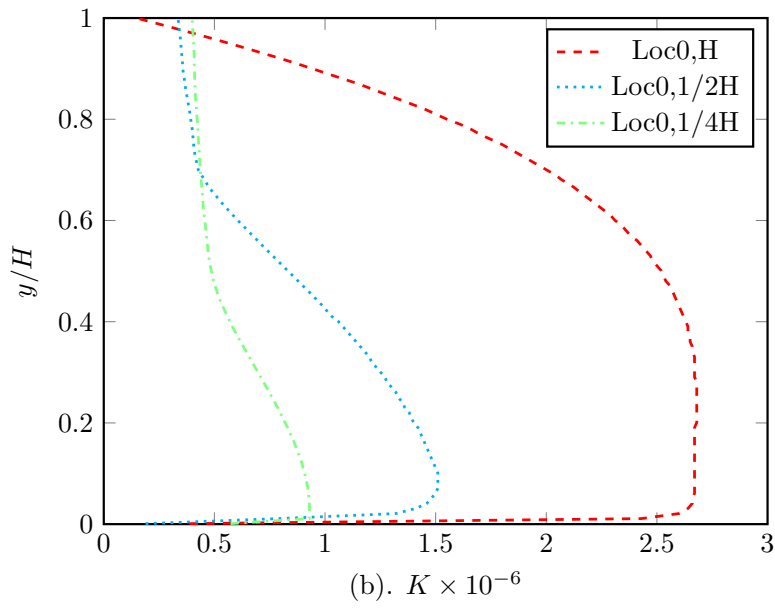
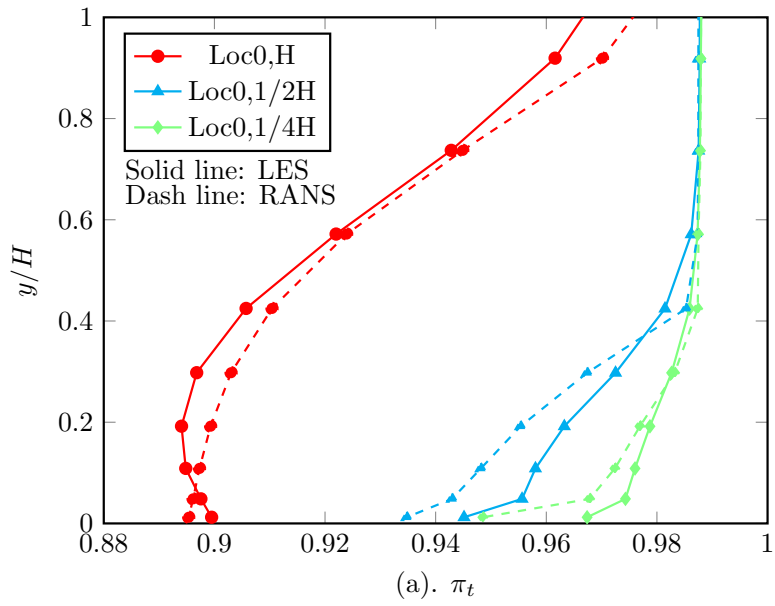


Fig. 14: Radial distributions of (a) total pressure ratio (b) acceleration parameter (c) angle of incidence predicted by RANS and LES at $x = 4.5H$. Cases compared for same fan location, Loc0 and varying beam heights: H, H/2, H/4.

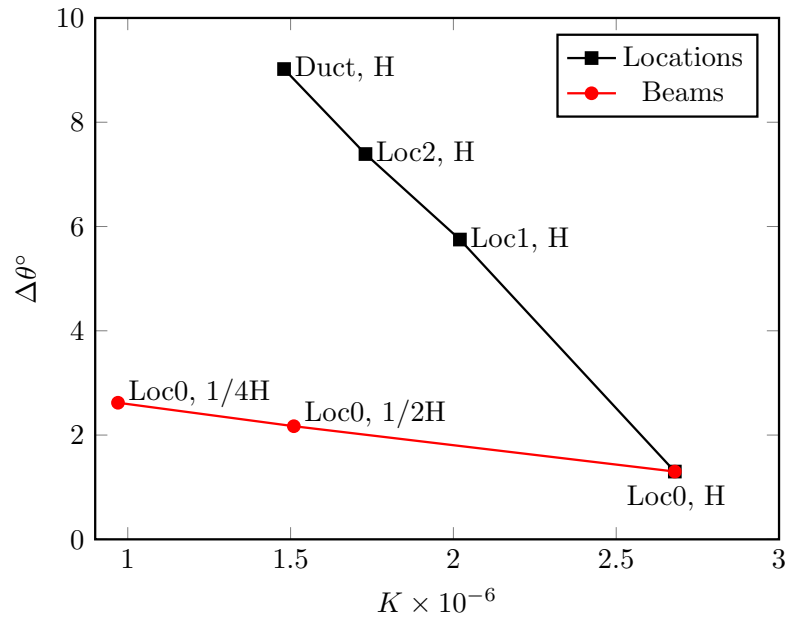


Fig. 15: Variation of maximum discrepancy in dtheta (typically observed at the casing) with acceleration parameter for all the test cases with varying fan-locations and beam heights

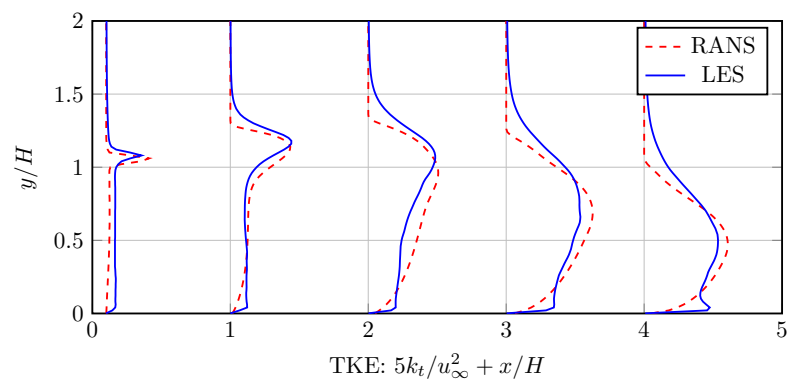


Fig. 16: Carpet plot comparing the prediction of TKE from LES against k-omega SST model for case Loc0, H

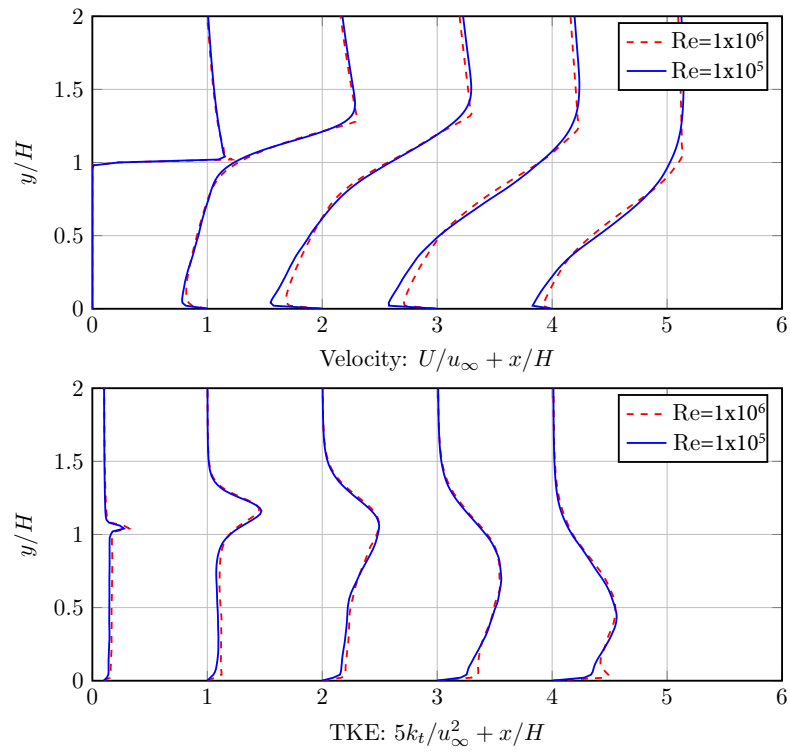


Fig. 17: Carpet plot showing LES predictions of (a) velocity profiles and (b) TKE profiles at two different Reynolds numbers for case Loc0, H